

# Close-packed layer spacing as a practical guideline for structure symmetry manipulation of IV-VI/I-V-VI<sub>2</sub> thermoelectrics

Tao Jin | Long Yang | Xinyue Zhang | Wen Li | Yanzhong Pei 

Interdisciplinary Materials Research Center, School of Materials Science and Engineering, Tongji University, Shanghai, the People's Republic of China

## Correspondence

Wen Li and Yanzhong Pei, Interdisciplinary Materials Research Center, School of Materials Science and Engineering, Tongji University, 4800 Caoan Rd., Shanghai 201804, the People's Republic of China.  
Email: [liwen@tongji.edu.cn](mailto:liwen@tongji.edu.cn); [yanzhong@tongji.edu.cn](mailto:yanzhong@tongji.edu.cn)

## Funding information

National Key Research and Development Program of China, Grant/Award Number: 2022YFA1203600; National Natural Science Foundation of China, Grant/Award Numbers: 51772215, 52022068, 52102292, T2125008; Innovation Program of Shanghai Municipal Education Commission, Grant/Award Number: 2021-01-07-00-07-E00096; Fundamental Research Funds for the Central Universities

## Abstract

The crystal-structure symmetry in real space can be inherited in the reciprocal space, making high-symmetry materials the top candidates for thermoelectrics due to their potential for significant electronic band degeneracy. A practical indicator that can quantitatively describe structural changes would help facilitate the advanced thermoelectric material design. In face-centered cubic structures, the spatial environment of the same crystallographic plane family is isotropic, such that the distances between the close-packed layers can be derived from the atomic distances within the layers. Inspired by this, the relationship between inter- and intra-layer geometric information can be used to compare crystal structures with their desired cubic symmetry. The close-packed layer spacing was found to be a practical guideline of crystal structure symmetry in IV-VI chalcogenides and I-V-VI<sub>2</sub> ternary semiconductors, both of which are historically important thermoelectrics. The continuous structural evolution toward high symmetry can be described by the layer spacing when temperature or/and composition change, which is demonstrated by a series of pristine and alloyed thermoelectric materials in this work. The layer-spacing-based guideline provides a quantitative pathway for manipulating crystal structures to improve the electrical and thermal properties of thermoelectric materials.

## KEYWORDS

phase transition, structure manipulation, thermoelectric materials, x-ray diffraction

## 1 | INTRODUCTION

Thermoelectric materials can convert electricity and heat without generating hazardous emissions or relying on moving parts, which have great potential for clean energy applications.<sup>1,2</sup> Nowadays, a significant obstacle impeding the application of thermoelectric devices is the low conversion

efficiency, which is determined by the dimensionless thermoelectric figure of merit,  $zT = S^2\sigma T / (\kappa_E + \kappa_L)$ , where  $T$ ,  $S$ ,  $\sigma$ ,  $\kappa_E$ , and  $\kappa_L$  are the temperature, Seebeck coefficient, electrical conductivity, and the electronic and lattice components of the thermal conductivity, respectively.<sup>3,4</sup>

Band engineering has been widely applied as an effective strategy for improving the thermoelectric properties.<sup>5-8</sup> The band structure determines the electrical characteristics of thermoelectrics. We expect the band structure to exhibit

Tao Jin and Long Yang contributed equally to this study.

This is an open access article under the terms of the [Creative Commons Attribution](https://creativecommons.org/licenses/by/4.0/) License, which permits use, distribution and reproduction in any medium, provided the original work is properly cited.

© 2023 The Authors. *InfoMat* published by UESTC and John Wiley & Sons Australia, Ltd.

a high band degeneracy, but low effective mass and deformation potential coefficient.<sup>9–11</sup> However, regulating the effective mass and the deformation potential coefficient are challenging tasks. One of the primary approaches is by increasing the electronic band degeneracy. Higher band degeneracy can significantly enhance the electrical conductivity without compromising the Seebeck coefficient.<sup>12</sup> Moreover, high band degeneracy is more likely to occur in high-symmetry crystal structures due to the inherent relationship with the reciprocal-space electronic structure. This has been validated by numerous cubic-structure thermoelectric materials, such as Si-Ge,<sup>13</sup> (Pb, Sn)Te,<sup>6,9</sup> PbSe,<sup>14–17</sup> Mg<sub>2</sub>Si,<sup>18–20</sup> CoSb<sub>3</sub>,<sup>21,22</sup> Cu<sub>2</sub>(Se, S),<sup>23</sup> AgSbTe<sub>2</sub>,<sup>24</sup> La<sub>3</sub>Te<sub>4</sub>,<sup>25</sup> clathrates,<sup>26</sup> and half-Heuslers.<sup>27</sup>

More recently, high band degeneracy has been achieved in rhombohedral GeTe by tuning its crystal structure.<sup>12</sup> The rhombohedral GeTe structure can be viewed as slightly elongated along the [111] crystallographic axis from its cubic phase. This leads to exceptional thermoelectric performance due to the degeneracy of a few symmetric electronic orbitals. Therefore, tuning the atomic structure to obtain desired symmetry can be an effective strategy for enhancing the band degeneracy and performance.

The crystal structure manipulation has been extensively applied for enhancing the thermoelectric properties by the solid solution of different systems.<sup>12,28–32</sup> However, a conclusive guideline for the crystal structure evolution remains unclear in this field. The general explanation of the crystal structure evolution is that solid solution of different atom species increases the conformational entropy,<sup>33,34</sup> or equivalently, reduces formation enthalpy.<sup>35</sup> However, the entropy- and enthalpy-based thermodynamic parameters are challenging to be implemented as practical experimental guidelines for tuning crystal structures.

In this work, the presence of close-packed layers within group IV-VI chalcogenides and group I-V-VI<sub>2</sub> ternary semiconductors inspired us to propose a new perspective, “spacing of close-packed layers”, to precisely characterize the crystal-structure difference among these compounds. We suggest that the spacing between close-packed layers can effectively describe the transformation of crystal structures during temperature and/or composition variations across different crystal systems. By applying the layer spacing strategy, we can quantitatively manipulate the crystal structure into expected symmetry.

## 2 | CLASSIFICATION OF SYMMETRY BY CLOSE-PACKED LAYER SPACING

Many IV-VI/I-V-VI<sub>2</sub> compounds undergo phase transitions by changing the temperature or by solid solution.

The lattice parameters, a common language that people usually use for describing crystal structures, can be quite different when the crystal symmetry changes. For example, rhombohedral and cubic GeTe unit cells have distinct lattice constants. However, the transition from one crystal structure to another is usually accompanied by subtle atomic displacements in the material. Therefore, different physical parameters other than lattice constants may provide a quantitative method to describe how structure changes during the phase transition. In the GeTe system, specifically, the interaxial angle is used to describe the rhombohedral crystal symmetry, and if it is closer to 90°, the structure gets closer to the cubic case. However, the interaxial angle cannot be applied to different crystal systems. Thus, a practical indicator for a broad range of material systems is needed for accurately describing the crystal structure evolution.

Group IV-VI chalcogenides and group I-V-VI<sub>2</sub> ternary semiconductors have aroused lots of research interests in recent years, due to their potential high-performance thermoelectric properties. Materials within these systems have diverse structural symmetries, which may enable the optimization of band structure via crystal structure manipulation. Within these groups, the trigonal and cubic crystal systems have a three-fold rotation or rotation-inversion axis. This results in atoms being closely packed in planes perpendicular to the principal axis to form close-packed layers. Consequently, these crystal structures are built up in an ABC-type atomic dense stacking (close-packed structure, as shown in Figure 1B). A similar atomic stacking can also be found in some low-symmetry materials, such as GeSe (space group: *Pnma*) and SnSe (s.g.: *Pnma*), which is shown in Figure S1 and discussed in more details in the Data S1. Here we propose a quantitative indicator of crystal symmetry based on the spacing between close-packed layers, which may serve as a practical guideline for manipulating crystal structures.

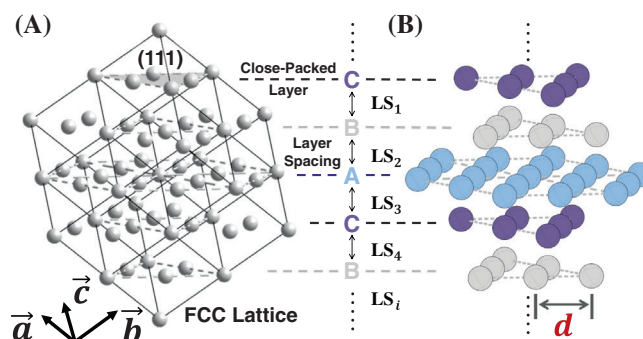


FIGURE 1 Schematic diagram of (A) the FCC lattice, and (B) the ABC-type dense stacking.

For a face-centered cubic (FCC) lattice, atoms are arranged in an ABC-type dense stacking along the close-packed direction, and the distance between the close-packed layers can be derived from atomic distances within layers. As depicted in Figure 1A, {111} crystallographic planes are close-packed layers, consisting of close-packed atoms. These atom layers are stacked in an ABC-type atomic arrangement perpendicular to the close-packed (111) layer. The spatial intervals between adjacent close-packed atomic layers are labeled as the “layer spacing” (LS). This parameter, for a FCC cubic lattice of elementary substances, can be calculated as  $\sqrt{6}/3$  times the neighboring atomic distance  $d$  (labeled in red in Figure 1B) within close-packed layers (i.e.,  $LS = \sqrt{6}/3d$ ).

Following the layer spacing definition in elementary substances, we can identify analogous layer spacings in group IV-VI and I-V-VI<sub>2</sub> compounds. For non-cubic materials listed in Table S1, there can be various layer spacings with different values, since their crystal structures do not strictly follow the close-packed stacking as in a cubic case. The various layer spacings are averaged to obtain the “average layer spacing” ( $LS_{\text{avg}}$ ), which is used to characterize the overall structural geometry. Subsequently, the distance between neighboring atoms in the close-packed atomic layer (labeled as red  $d$  in Figure 1B) is used for determining the equivalent layer spacing of the corresponding cubic symmetry. Likewise, the “cubic layer spacing” ( $LS_{\text{cub}} = \sqrt{6}/6d$  for compounds listed in Table S1) is considered as a standard reference when comparing with the “average layer spacing” across different crystal systems. Note that  $LS_{\text{cub}}$  is for reference purpose only and may not necessarily be the same as the cubic structure for materials undergoing a phase transition to cubic phase. Considering the difference between elementary substances and compounds, which are composed of alternating anion and cation layers along the close-packed direction, we refer layer spacing  $LS_i$  as the spacing between adjacent layers (such as the spacing between anion and cation layers for IV-VI binary and I-V-VI<sub>2</sub> ternary semiconductors, as shown in Figure 2). For compounds, the calculation of  $LS_{\text{cub}}$  would be half of that in the case of elementary substance.

It is crucial to underscore that the discussions are focused on crystal structures with ABC-type dense stacking arrangements, where anionic and cationic layers are stacked on top of each other. The layer spacing is suitable for characterizing the crystal structures of most IV-VI chalcogenides, I-V-VI<sub>2</sub> ternary semiconductors and their alloys that contain the same number of cations and anions in the system. For other systems, such as the V<sub>2</sub>-VI<sub>3</sub> group thermoelectrics, when alloying with IV-VI chalcogenides, the cation-to-anion ratio will inevitably introduce large amounts of vacancies. This could lead to complex

situations, such as forming van der Waals interactions, which are beyond the discussions of the current work.

To indicate how the crystal structure deviates from the high-symmetry cubic structure, we compare the average layer spacing of the solid solution material studied with the corresponding cubic layer spacing. In this way, materials can be classified into three categories depending on how they deviate from the cubic symmetry reference: crystal symmetry with positive deviation from the cubic structure ( $LS_{\text{avg}} > LS_{\text{cub}}$ ); materials with cubic structure ( $LS_{\text{avg}} = LS_{\text{cub}}$ ); and crystal symmetry with negative deviation from the cubic structure ( $LS_{\text{avg}} < LS_{\text{cub}}$ ). In the following, each of these three categories will be introduced individually.

For crystal symmetry with positive deviation ( $LS_{\text{avg}} > LS_{\text{cub}}$ ), take the room-temperature rhombohedral GeTe (Figure 2A, s.g.:  $R3m$ , ICSD Collection Code: 101817, whose crystal structure is determined at 293 K)<sup>36</sup> as an example, the close-packed layer of its crystal structure corresponds to the (001) planes with two types of layer spacing ( $LS_1$  and  $LS_2$ ). The average layer spacing is 1.78 Å and the equivalent cubic layer spacing is 1.70 Å. Thus,  $LS_{\text{avg}}/LS_{\text{cub}} = 104.6\%$  at room temperature, providing a quantitative representation of the symmetry deviation from cubic (i.e., a positive deviation of 4.6%).

For the cubic structured materials, they have close-packed (111) planes with the same layer spacing. For example, in the high-temperature cubic GeTe (Figure 2B, s.g.:  $Fm\bar{3}m$ , ICSD Collection Code: 602124, whose crystal structure is determined at 773 K)<sup>37</sup> or cubic AgBiSe<sub>2</sub> (Figure 2D, s.g.:  $Fm\bar{3}m$ , ICSD Collection Code: 604858),<sup>38</sup> all layer spacings between (111) planes are the same, equivalent to the cubic layer spacing ( $LS_{\text{avg}} = LS_{\text{cub}} = \sqrt{6}/6d$ , thus  $LS_{\text{avg}}/LS_{\text{cub}} = 100\%$ ).

AgBiS<sub>2</sub>, AgBiSe<sub>2</sub>, and AgBiTe<sub>2</sub> have been found to exhibit negative deviations ( $LS_{\text{avg}} < LS_{\text{cub}}$ ), and the last one is thermodynamically unstable at room temperature. Take AgBiSe<sub>2</sub> as an example, the room-temperature trigonal AgBiSe<sub>2</sub> (Figure 2C, s.g.:  $P\bar{3}m1$ , ICSD Collection Code: 7661, whose crystal structure is determined at 293 K)<sup>39</sup> has six different layer spacings for close-packed (001) planes. The average layer spacing is 1.64 Å and the equivalent cubic layer spacing is 1.71 Å, which gives  $LS_{\text{avg}}/LS_{\text{cub}} = 95.7\%$ , indicating a negative deviation of 4.3%.

### 3 | VALIDATING THE LAYER SPACING GUIDELINE FOR PHASE TRANSITION

Layer spacing can be used as a practical indicator for symmetry change, and it varies smoothly across different crystal

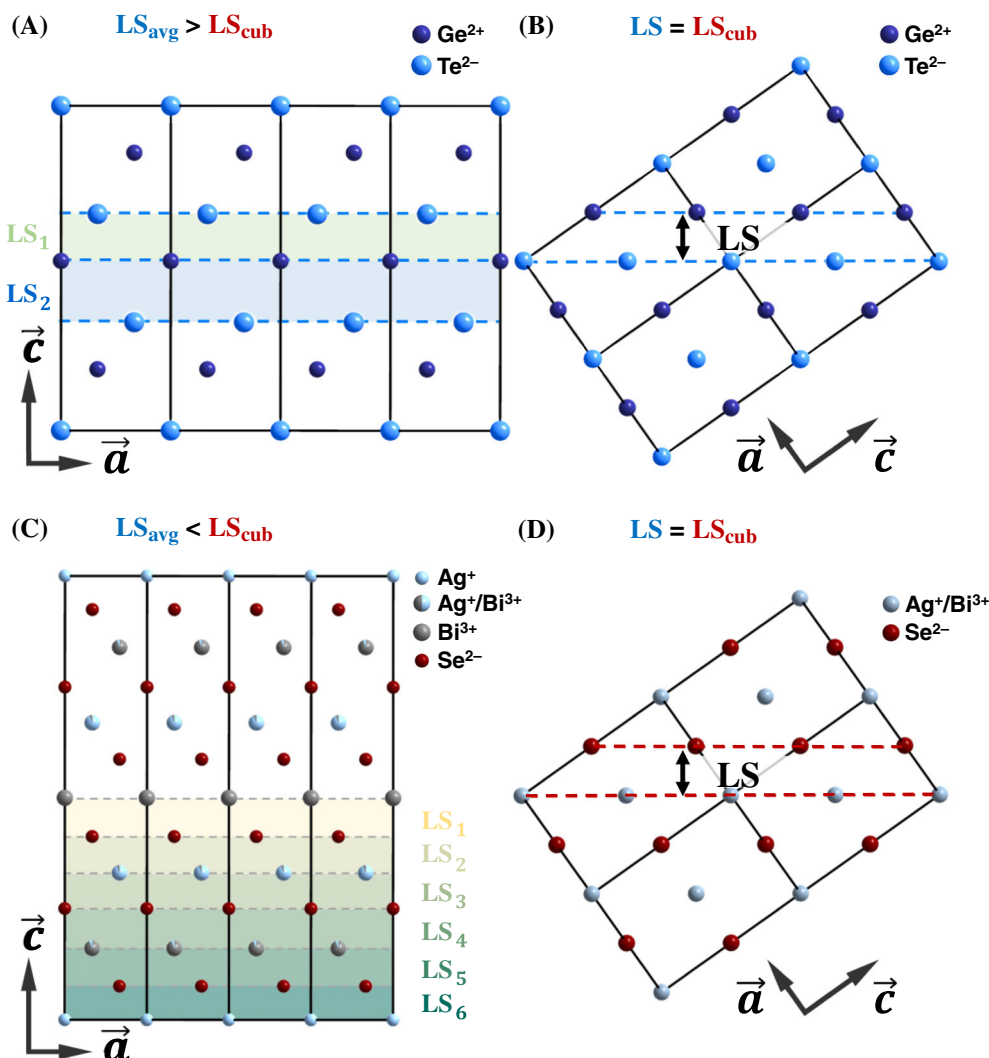


**FIGURE 2** Schematic diagrams for the close-packed layer spacing of materials with different deviations from cubic symmetry. (A) The room-temperature rhombohedral GeTe ( $R\bar{3}m$ ),  $4 \times 1 \times 1$  supercell, (C) the room-temperature trigonal AgBiSe<sub>2</sub> ( $P\bar{3}m1$ ),  $4 \times 1 \times 1$  supercell and the high-temperature cubic (B) GeTe ( $Fm\bar{3}m$ ) and (D) AgBiSe<sub>2</sub> ( $Fm\bar{3}m$ ),  $2 \times 1 \times 1$  supercells. The dotted lines indicate the “close-packed layers”.

symmetries. According to the results for IV-VI and I-V-VI<sub>2</sub> materials summarized in Table S1, for a given material with temperature-dependent phase transition, the layer spacing ratio ( $LS_{avg}/LS_{cub}$ ) varies continuously across different space groups. Therefore, we expect that the phase transition could potentially be guided by the layer spacing ratio ( $LS_{avg}/LS_{cub}$ ).

To verify this, GeTe and AgBiSe<sub>2</sub> that exhibit a temperature-induced phase transition from a low-temperature low symmetry to a high-temperature cubic phase were studied by XRD measurements on warming. In Figure S2, GeTe transforms from a rhombohedral phase at room temperature to a cubic phase at high temperature. Similarly, as the temperature increases, AgBiSe<sub>2</sub> transforms from a trigonal phase at room temperature to a cubic phase at high temperature. The two characteristic peaks over the  $2\theta = 40^\circ$ – $45^\circ$  region gradually merge into

one single peak on warming, which is consistent with the phase transitions reported in previous studies.<sup>28,40,41</sup>

To quantitatively investigate the crystal structure transition, the Rietveld refinements were performed on the XRD data to study the changes of layer spacing on warming (Figure S3). The layer spacing ratio  $LS_{avg}/LS_{cub}$  (Figure 3) was derived from the refined structure to describe how the crystal structure approaches the high-symmetry cubic structure on warming. In the case of positively deviated GeTe, the layer spacing ratio decreases to 100% as temperature increases, indicated by the blue solid line in Figure 3. This trend signifies a gradual convergence toward the cubic structure. Conversely, for negatively deviated AgBiSe<sub>2</sub>, the layer spacing ratio gradually increases to 100%, as indicated by the purple solid line in Figure 3.

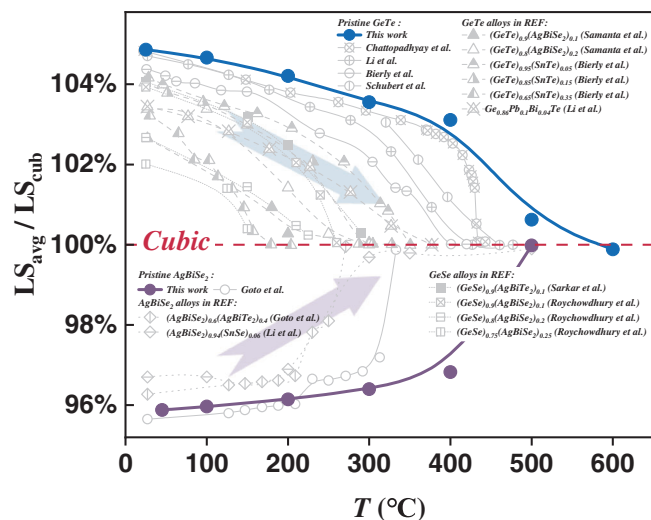


**FIGURE 3** The relationship between the close-packed layer spacing ratio ( $LS_{\text{avg}}/LS_{\text{cub}}$ ) and temperature for IV-VI and I-V-VI<sub>2</sub> compounds when the temperature changes.

The structure information reported in the literatures are collected systemically and the layer spacing ratio ( $LS_{\text{avg}}/LS_{\text{cub}}$ ) is calculated accordingly, shown in the gray lines of Figure 3, which aligns with the smooth transition trend toward cubic structure on warming, as observed in our work.<sup>12,28–30,36,42–44</sup> This further supports the close-packed layer spacing as a practical guideline for understanding the temperature induced phase transition in IV-VI and I-V-VI<sub>2</sub> compounds.

#### 4 | SYMMETRY MANIPULATION GUIDED BY LAYER SPACING

As the crystal structure of materials gradually approaches the cubic symmetry, the layer spacing ratio ( $LS_{\text{avg}}/LS_{\text{cub}}$ ) converges toward 100%, which provides a quantitative indicator for describing crystal structures. Thus, a solid solution of positively and negatively deviated materials is expected to enable precise manipulation of crystal structure in a straightforward manner.

GeTe, GeSe, and SnSe were chosen as the positively deviated materials, and on the other hand, AgBiSe<sub>2</sub> and AgBiTe<sub>2</sub> were selected as the negatively deviated ones. Following the layer spacing guideline, the structure of alloys can transform from the pristine low-symmetry phase (trigonal or rhombohedral in this case) to the cubic structure.

The relationship between the layer spacing ratio ( $LS_{\text{avg}}/LS_{\text{cub}}$ ) and solid solution composition of these alloys is plotted as colored solid lines in Figure 4. Obviously, the layer spacing ratio gradually increases from <100% to 100% as dissolving positively deviated

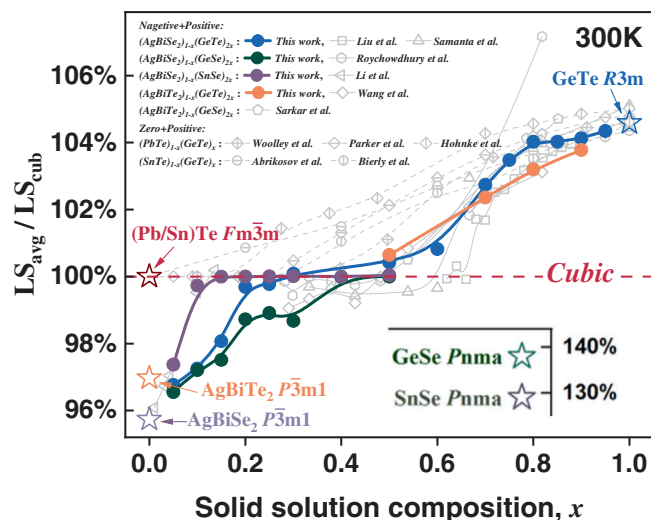


**FIGURE 4** The relationship between the close-packed layer spacing ratio ( $LS_{\text{avg}}/LS_{\text{cub}}$ ) and composition for IV-VI and I-V-VI<sub>2</sub> solid solutions when the composition ratio  $x$  changes.

materials (GeTe, GeSe, SnSe) into negatively deviated materials (AgBiSe<sub>2</sub>), which means structures approach the cubic symmetry. In addition, when the concentration of GeTe in AgBiSe<sub>2</sub> or AgBiTe<sub>2</sub> increases, the layer spacing ratio gradually increases to that of pristine GeTe.

Literature results on solid solutions with the combinations of “negative + positive” and “zero + positive” layer spacing ratios were also included as gray symbols in Figure 4.<sup>28–30,36,41,43,45–48</sup> As the solid solution composition varies, the structural symmetry evolves gradually, which can be well understood by the “compensation” of deviations in the close-packed layer spacing ratio.

Our results suggest that layer spacing can serve as a guiding factor in manipulating crystal structures, with the potential to enhance thermoelectric performance. However, it is important to note that while adjusting the crystal structure is a potential strategy for improving thermoelectric performance, it does not guarantee superior performance universally. The electrical properties have a close relationship with crystal structures, yet they can also be influenced by various complicated factors, including spin-orbit coupling and additional scattering introduced by solid-solution. Nevertheless, the structural symmetry could be one of the fundamentals determining the phononic and electronic structures. For instance, the chemical bonding and coordination environment, which are directly adjusted by crystal structures, would play important roles in determining the degree of anharmonicity in lattice vibrations, thus affecting the lattice thermal conductivity. In addition, high-symmetry structures in real space increase the probability of

forming highly degenerate electronic band structures that give rise to the electrical conductivity without the loss of Seebeck coefficient.<sup>12</sup> For the IV-VI and I-V-VI<sub>2</sub> families under study, the property measurements show that either the resistivity, the Seebeck coefficient or the lattice thermal conductivity have been significantly manipulated in (GeTe)<sub>1-x</sub>(Ag<sub>0.5</sub>Bi<sub>0.5</sub>Se)<sub>x</sub> (Figure S5). Therefore, the layer spacing strategy remains a valuable quantitative indicator for tuning crystal structures, potentially leading to well-improved thermoelectric performance in the near future.

## 5 | CONCLUSION

With the insight of inherently existing close-packed atomic layers in IV-VI/I-V-VI<sub>2</sub> thermoelectrics, this work introduces a classification rule to understand the crystal symmetry evolution induced by either temperature or composition variations. The existence of both positively and negatively deviated structures from cubic symmetry within these materials provides the possibility, not only to precisely design new crystal structures with desired symmetry and thus band degeneracy for efficient thermoelectrics, but also to understand the linkage between real-space atomic structure and reciprocal-space electronic structure in existing studies. The layer spacing indicator is, therefore, a quantitative practical guideline for symmetry manipulation and thus for improving functionality for IV-VI/I-V-VI<sub>2</sub> compounds/alloys.

## 6 | EXPERIMENTAL SECTION

In this work, samples of two pristine systems and four solid solution systems were synthesized, which were GeTe, AgBiSe<sub>2</sub>, (AgBiSe<sub>2</sub>)<sub>1-x</sub>(GeTe)<sub>2x</sub> ( $x = 0.05, 0.1, 0.15, 0.2, 0.25, 0.3, 0.5, 0.6, 0.7, 0.75, 0.8, 0.85, 0.9, 0.95$ ), (AgBiSe<sub>2</sub>)<sub>1-x</sub>(SnSe)<sub>2x</sub> ( $x = 0.05, 0.1, 0.15, 0.2, 0.25, 0.3, 0.4, 0.5$ ), (AgBiSe<sub>2</sub>)<sub>1-x</sub>(GeSe)<sub>2x</sub> ( $x = 0.05, 0.1, 0.15, 0.2, 0.25, 0.3, 0.4, 0.5$ ), and (AgBiTe<sub>2</sub>)<sub>1-x</sub>(GeTe)<sub>2x</sub> ( $x = 0.5, 0.7, 0.8, 0.9$ ). The elements weighed according to the stoichiometry were sealed in vacuum quartz tubes, heated to 1000°C in 7.5 h and held for about 6 h. They were then quenched and annealed for 1 day and cooled with the furnace. The purity of all the elements used to synthesize the samples was higher than 99.99%. For x-ray powder diffraction (XRD) experiments, the ingots obtained were ground into fine powders that passed through a 600-mesh sieve. All powder samples were characterized by D8 Advance (BRUKER) with Cu K $\alpha$  radiation  $\lambda = 1.5406 \text{ \AA}$ .

The Rietveld refinements of the XRD data were carried out by the GSAS-II software.<sup>49</sup> The refined crystal structures were then exported and relevant spatial

information was calculated from them. All crystallographic information files (CIFs) used for structural modeling and calculations are from the Inorganic Crystal Structure Database (ICSD).<sup>50,51</sup>

Bulk samples were obtained by an induction heating hot press system at 793 K for 40 min under a uniaxial pressure of  $\sim 80$  MPa. The resistivity was measured using the van der Pauw technique. The Seebeck coefficient was obtained from the slope of the thermopower versus temperature gradients within 0–5 K. The thermal conductivity was calculated by  $\kappa = dC_pD$ , where  $d$  is the density obtained by Archimedes method,  $C_p$  is the heat capacity estimated by the Dulong–Petit approximation and is assumed to be temperature independent,  $D$  is the thermal diffusivity measured by a laser flash technique (Netzsch LFA467 system). The uncertainty of measurements of  $S$ ,  $\rho$ , and  $D$  is about 5%.

## ACKNOWLEDGMENTS

This work is supported by the National Key Research and Development Program of China (2022YFA1203600), the National Natural Science Foundation of China (Grant No. T2125008, 51772215, 52022068, 52102292), the Innovation Program of Shanghai Municipal Education Commission (2021-01-07-00-07-E00096), the Fundamental Research Funds for the Central Universities.

## CONFLICT OF INTEREST STATEMENT

The authors declare no conflict of interest.

## ORCID

Yanzhong Pei  <https://orcid.org/0000-0003-1612-3294>

## REFERENCES

- Mori T. Novel principles and nanostructuring methods for enhanced thermoelectrics. *Small*. 2017;13(45):1702013.
- Bell LE. Cooling, heating, generating power, and recovering waste heat with thermoelectric systems. *Science*. 2008; 321(5895):1457-1461.
- Zhu T, Liu Y, Fu C, Heremans JP, Snyder JG, Zhao X. Compromise and synergy in high-efficiency thermoelectric materials. *Adv Mater*. 2017;29(14):1605884.
- Goldsmid HJ. *Introduction to Thermoelectricity*. Vol 121. Springer; 2016.
- Pei YZ, Wang H, Snyder GJ. Band engineering of thermoelectric materials. *Adv Mater*. 2012;24(46):6125-6135.
- Pei YZ, Shi XY, LaLonde A, Wang H, Chen LD, Snyder GJ. Convergence of electronic bands for high performance bulk thermoelectrics. *Nature*. 2011;473(7345):66-69.
- Lin SQ, Li W, Chen ZW, Shen JW, Ge BH, Pei YZ. Tellurium as a high-performance elemental thermoelectric. *Nat Commun*. 2016;7(1):7.
- Heremans JP, Jovovic V, Toberer ES, et al. Enhancement of thermoelectric efficiency in PbTe by distortion of the electronic density of states. *Science*. 2008;321(5888):554-557.

9. Li W, Zheng LL, Ge BH, et al. Promoting SnTe as an eco-friendly solution for p-PbTe thermoelectric via band convergence and interstitial defects. *Adv Mater.* 2017;29(17):29.
10. Pei YZ, LaLonde AD, Wang H, Snyder GJ. Low effective mass leading to high thermoelectric performance. *Energ Environ Sci.* 2012;5(7):7963.
11. Wang H, Pei YZ, LaLonde AD, Snyder GJ. Weak electron-phonon coupling contributing to high thermoelectric performance in n-type PbSe. *Proc Natl Acad Sci U S A.* 2012;109(25):9705-9709.
12. Li J, Zhang XY, Chen ZW, et al. Low-symmetry rhombohedral GeTe thermoelectrics. *Joule.* 2018;2(5):976-987.
13. Vining CB. *CRC Handbook of Thermoelectrics.* CRC Press; 1995:329.
14. Kim SI, Lee KH, Mun HA, et al. Dense dislocation arrays embedded in grain boundaries for high-performance bulk thermoelectrics. *Science.* 2015;348(6230):109-114.
15. Chen Z, Ge B, Li W, et al. Vacancy-induced dislocations within grains for high-performance PbSe thermoelectrics. *Nat Commun.* 2017;8(1):13828.
16. Xin J, Wu H, Liu X, Zhu T, Yu G, Zhao X. Mg vacancy and dislocation strains as strong phonon scatterers in  $\text{Mg}_2\text{Si}_{1-x}\text{Sb}_x$  thermoelectric materials. *Nano Energy.* 2017;34:428-436.
17. Carruthers P. Scattering of phonons by elastic strain fields and the thermal resistance of dislocations. *Phys Rev.* 1959;114(4):995-1001.
18. Liu W, Tan XJ, Yin K, et al. Convergence of conduction bands as a means of enhancing thermoelectric performance of n-Type  $\text{Mg}_2\text{Si}_{1-x}\text{Sn}_x$  solid solutions. *Phys Rev Lett.* 2012;108:166601.
19. Cheng K, Bu ZL, Tang J, et al. Efficient  $\text{Mg}_2\text{Si}_{0.3}\text{Sn}_{0.7}$  thermoelectrics demonstrated for recovering heat of about 600 K. *Mater Today Phys.* 2022;28:100887.
20. Liu X, Zhu T, Wang H, et al. Low electron scattering potentials in high performance  $\text{Mg}_2\text{Si}_{0.45}\text{Sn}_{0.55}$  based thermoelectric solid solutions with band convergence. *Adv Energy Mater.* 2013;3(9):1238-1244.
21. Tang YL, Gibbs ZM, Agapito LA, et al. Convergence of multi-valley bands as the electronic origin of high thermoelectric performance in  $\text{CoSb}_3$  skutterudites. *Nat Mater.* 2015;14(12):1223-1228.
22. Kajikawa Y. Refined analysis of the transport properties of  $\text{Co}_1\text{-NiSb}_3$  according to a model including a deep donor level and the second lowest valleys of the conduction band. *J Alloys Compd.* 2015;621:170-178.
23. Tyagi K, Gahtori B, Bathula S, Auluck S, Dhar A. Band structure and transport studies of copper selenide: an efficient thermoelectric material. *Appl Phys Lett.* 2014;105(17):105.
24. Barabash S, Ozolins V. Order, miscibility, and electronic structure of  $\text{Ag}(\text{Bi,Sb})\text{Te}_2$  alloys and  $(\text{Ag,Bi,Sb})\text{Te}$  precipitates in rocksalt matrix: a first-principles study. *Phys Rev B.* 2010;81(7):075212.
25. May AF, Flage-Larsen E, Snyder GJ. Electron and phonon scattering in the high-temperature thermoelectric  $\text{La}_3\text{Te}_{4-z}\text{M}_z$  ( $\text{M} = \text{Sb,Bi}$ ). *Phys Rev B.* 2010;81(12):125205.
26. Wunderlich W, Amano M, Matsumura Y. Electronic band-structure calculations of  $\text{Ba}_8\text{Me}_x\text{Si}_{46-x}$  clathrates with  $\text{me} = \text{Mg, Pd, Ni, Au, Ag, Cu, Zn, Al, Sn}$ . *J Electron Mater.* 2014;43(6):1527-1532.
27. Fu C, Bai S, Liu Y, et al. Realizing high figure of merit in heavy-band p-type half-Heusler thermoelectric materials. *Nat Commun.* 2015;6(1):8144.
28. Li S, Hou S, Xue W, et al. Manipulation of phase structure and Se vacancy to enhance the average thermoelectric performance of  $\text{AgBiSe}_2$ . *Mater Today Phys.* 2022;27:100837.
29. Sarkar D, Roychowdhury S, Arora R, et al. Metavalent bonding in GeSe leads to high thermoelectric performance. *Angew Chem Int ed.* 2021;60(18):10350-10358.
30. Roychowdhury S, Ghosh T, Arora R, Waghmare UV, Biswas K. Stabilizing n-type cubic GeSe by entropy-driven alloying of  $\text{AgBiSe}_2$ : ultralow thermal conductivity and promising thermoelectric performance. *Angew Chem Int Ed.* 2018;57(46):15167-15171.
31. Chandra S, Arora R, Waghmare UV, Biswas K. Modulation of the electronic structure and thermoelectric properties of orthorhombic and cubic SnSe by  $\text{AgBiSe}_2$  alloying. *Chem Sci.* 2021;12(39):13074-13082.
32. Liu H-X, Zhang X-Y, Bu Z-L, Li W, Pei Y-Z. Thermoelectric properties of  $(\text{GeTe})_{1-x}[(\text{Ag}_2\text{Te})_{0.4}(\text{Sb}_2\text{Te}_3)_{0.6}]_x$  alloys. *Rare Metals.* 2022;41(3):921-930.
33. Zhao T, Yang L-Z, Zhou Y, et al. Thermoelectric performance of  $(\text{AgBiTe}_2)_{1-x}(\text{SnTe})_x$  with stable cubic enabled by enhanced configurational entropy. *Rare Metals.* 2022;41(12):4149-4155.
34. Luo Y, Hao S, Cai S, et al. High thermoelectric performance in the new cubic semiconductor  $\text{AgSnSbSe}_3$  by high-entropy engineering. *J Am Chem Soc.* 2020;142(35):15187-15198.
35. Yan M, Geng H, Jiang P, Bao X. Glass-like electronic and thermal transport in crystalline cubic germanium selenide. *J Energy Chem.* 2020;45:83-90.
36. Samanta M, Ghosh T, Arora R, Waghmare UV, Biswas K. Realization of both n- and p-type GeTe thermoelectrics: electronic structure modulation by  $\text{AgBiSe}_2$  alloying. *J Am Chem Soc.* 2019;141(49):19505-19512.
37. Shu HW, Jaulmes S, Ollitrault-Fichet R, Flahaut J. Système As-Ge-Te. *J Solid State Chem.* 1987;69(1):48-54.
38. Glatz AC, Pinella A. X-ray and neutron diffraction studies of the high-temperature-phase of the  $\text{AgBiSe}_2/\text{AgBiS}_2$  system. *J Mater Sci.* 1968;3(5):498-501.
39. Böcher F, Culver SP, Peilstöcker J, Weldert KS, Zeier WG. Vacancy and anti-site disorder scattering in  $\text{AgBiSe}_2$  thermoelectrics. *Dalton Trans.* 2017;46(12):3906-3914.
40. Shuling W, Meng J, Lianjun W, Wan J. n-type Pb-free  $\text{AgBiSe}_2$  based thermoelectric materials with stable cubic phase structure. *J Inorg Mater.* 2023;38(7):807-814.
41. Liu H, Zhang X, Li J, et al. Band and phonon engineering for thermoelectric enhancements of rhombohedral GeTe. *ACS Appl Mater Interfaces.* 2019;11(34):30756-30762.
42. Chattopadhyay T, Boucherle JX, VonSchnering HG. Neutron diffraction study on the structural phase transition in GeTe. *J Phys C: Solid State Phys.* 1987;20(10):1431-1440.
43. Bierly JN, Muldrew L, Beckman O. The continuous rhombohedral-gubic transformation in GeTe-SnTe alloys. *Acta Metall.* 1963;11(5):447-454.
44. Goto Y, Nishida A, Nishiate H, et al. Effect of Te substitution on crystal structure and transport properties of  $\text{AgBiSe}_2$  thermoelectric material. *Dalton Trans.* 2018;47(8):2575-2580.
45. Wang D-Z, Liu W-D, Li M, et al. Hierarchical architectural structures induce high performance in n-type GeTe-based thermoelectrics. *Adv Funct Mater.* 2023;33(14):2213040.
46. Woolley JC, Nikolić PM. Some properties of GeTe-PbTe alloys. *J Electrochem Soc.* 1965;112(1):82.
47. Parker SG, Pinnell JE, Johnson RE. Growth of large crystals of (Pb,Ge)Te and (Pb,Sn)Te. *J Electron Mater.* 1974;3(4):731-746.

48. Hohnke DK, Holloway H, Kaiser S. Phase relations and transformations in the system PbTe-GeTe. *J Phys Chem Solid*. 1972; 33(11):2053-2062.
49. Toby BH, Von Dreele RB. GSAS-II: the genesis of a modern open-source all purpose crystallography software package. *J Appl Cryst*. 2013;46(2):544-549.
50. Bergerhoff G, Hundt R, Sievers R, Brown I. The inorganic crystal structure data base. *J Chem Inf Comput Sci*. 1983;23(2):66-69.
51. Belsky A, Hellenbrandt M, Karen VL, Luksch P. New developments in the inorganic crystal structure database (ICSD): accessibility in support of materials research and design. *Acta Crystallogr Sect B: Struct Sci*. 2002;58(3):364-369.

## SUPPORTING INFORMATION

Additional supporting information can be found online in the Supporting Information section at the end of this article.

**How to cite this article:** Jin T, Yang L, Zhang X, Li W, Pei Y. Close-packed layer spacing as a practical guideline for structure symmetry manipulation of IV-VI/I-V-VI<sub>2</sub> thermoelectrics. *InfoMat*. 2023;e12502. doi:[10.1002/inf2.12502](https://doi.org/10.1002/inf2.12502)